www.cadanda.com
Computer-Aided Design AND APPLICATIONS

An Ad-hoc Solution for Ear Anatomy Acquisition in Pediatric Setting

Michaela Servi[1], Elisa Mussi[2], Andrea Profili[3] and Yary Volpe[4]

[1] University of Florence, Italy, michaela.servi@unifi.it
[2]University of Florence, Italy, elisa.mussi@unifi.it
[3]University of Florence, Italy, andrea.profili@unifi.it
[4]University of Florence, Italy, yary.volpe@unifi.it

Corresponding author: Michaela Servi, michaela.servi@unifi.it

Abstract. Medical simulation tools have become increasingly popular in recent years for planning complex and non-routine surgeries. This applies also to autologous ear reconstruction, a procedure that is performed when patients have a complete or partial lack of the outer ear. On the basis of the contralateral ear, the physician sculpts a portion of costal cartilage that is then placed subcutaneously in the auricular region. Simulation tools can help the physician to familiarize with the specific geometries and shapes of the ear to be reconstructed. Making simulation tools requires the 3D acquisition of the ear, which can be done through optical scanners or diagnostic images (CT scan). This work focused on the development of a non-invasive, low-cost scanner for the acquisition of the outer ear. To this end, Intel RealSense D405 cameras were chosen, and a dedicated structure for the acquisition of ear anatomy was designed and manufactured, coupled with management software. The design of the scanner leveraged tests made with the Blender software for the optimization of the position and number of devices, while ensuring complete ear acquisition. Tests allowed the validation of the instrument both qualitatively, indicating the satisfaction of the medical staff in using the scanner, and quantitatively, measuring the deviation of the acquisition from a reference model obtained with professional scanners.

Keywords: Reverse Engineering, Optical Scanner, CAD Modelling, 3D Ear Acquisition.
DOI: https://doi.org/10.14733/cadaps.2023.S6.50-61

1 INTRODUCTION

The new paradigm of personalized medicine, increasingly applied in clinical practice for the fabrication of medical devices tailored to the patient's anatomy, has opened a new line of research dedicated to the development of 3D anatomy acquisition systems, which, integrated with Reverse Engineering (RE) and Additive Manufacturing (AM) technologies, enable the production of custom-

made medical devices [20,1]. Whereas traditional diagnostic tools such as CT and RX are still an important data source for anatomy acquisition, they have the disadvantage of subjecting the patient to ionizing radiation. An alternative technique for anatomy acquisition is the use of optical scanners [13,4]. In this way, the external geometry of the anatomical districts of interest can be obtained; the accuracy of the reconstructed geometry is closely related to the employed device. Professional scanners (such as Artec Spider, Minolta, Romer Absolute Arm) allow to reach accuracy values of less than a tenth of a millimeter, however, they have the disadvantage of being very expensive. Non-professional scanners (such as for example Structure Sensor, Intel RealSense family), although low-cost, are much less accurate and require several post-processing procedures in order to obtain data compliant with the clinical application. To optimize the anatomy acquisition phase, ad hoc scanners [4,12] have been developed in recent years, designed to be used in the clinical setting. The requirements of a scanner designed for the clinical setting typically are speed of acquisition, patient comfort, noninvasiveness, ease of use, and cost containment. Acquisition speed is essential in order to avoid artifacts given by subject movement during scanning, factors such as patient comfort, noninvasiveness of the device, and ease of use improve the physician and patient experience. Finally, cost containment makes ad hoc built scanners competitive in the marketplace and more easily inserted into public and nonpublic clinical settings. One of the areas that could benefit most from the introduction of ad hoc optical scanners is the pediatric field since the involved subjects exhibit high interindividual variability, may be uncooperative subjects, and in general it is difficult for a pediatric patient to maintain a position for longer than a few seconds. Consequently, the development of 3D optical scanners based on passive or active noninvasive technologies specifically designed for the acquisition of targeted anatomies, taking into account the aforementioned factors, could facilitate the application of high-quality personalized medicine procedures.

In this context, this paper proposes the development of an ad hoc scanner for the acquisition of the external auricular anatomy of pediatric patients. The need for a 3D model of the external ear arises when treating patients suffering from microtia [21], a congenital disorder consisting of the malformation or complete absence of the external ear. In these cases, the treatments considered to restore the anatomy can be 1) removable silicone prostheses [15], 2) reconstruction with autologous tissue [3] and 3) alloplastic implants made of Medpor [17]. In the first two cases, the missing or malformed geometry is reconstructed based on the geometry of the contralateral healthy ear, so anatomical acquisition is a first and fundamental step in the reconstruction process. Currently, the commonly used acquisition method for this purpose involves the use of CT imaging or the professional scanner Artec Spider [23], to which are associated disadvantages described above such as invasiveness, cost, etc. The scanner, presented in this paper, was designed with the aim of making a device that can be easily used in a hospital setting, optimizing the overall cost of the system and usability by healthcare users. The paper is organized as follows: Section 2 shows the steps that led to the realization of the scanner and the final device; Section 3 shows the testing campaign carried out by using the developed device; finally, in Section 4 the results are commented, and conclusions are drawn.

2 MATERIALS AND METHODS

Generally, the process of designing ad hoc scanners that take advantage of low-cost devices involves a number of considerations including (1) what type of 3D sensor is best suited to acquire the anatomy of interest; (2) how many cameras are needed to acquire the entire geometry and how to arrange the acquisition devices to scan larger and smaller anatomies; (3) how to acquire the 3D data as quickly as possible. In addition to these considerations, a number of constraints related to the use in the hospital environment come into play, such as (4) the handiness of the device; (5) the safety and ease of use of the hardware and software system.

Usually, these variables have to be considered in a waterfall design; in fact, each device has different field-of-view characteristics, thus a more or less wide acquisition of the scene, which affect the number of acquisitions required to be able to obtain the reproduction of the entire

anatomy of interest and the possible positioning and number of devices. Also depending on the chosen technology, it can be possible to reduce the acquisition time by following different strategies; in case, for instance, a structured light camera is chosen, overlapping light patterns will have to be avoided, for example by acquiring in a sequential way [4]. The achievable manageability depends on the size of the device, the number of required devices, and the chosen hardware configuration.

2.1 Device Choice

The acquisition device was chosen from low-cost RGB-D devices on the market, which are widely used in different fields such as fashion, medical, security, etc. [9,8]. Prominent in the current landscape are the devices of the Intel RealSense family [22,2,16,10]. These devices combine features of affordability, compactness, accuracy and programming freedom, which are very important for the development of ad hoc solutions. Among them, the authors' attention focused on two models: the Intel RealSense D415 camera and the Intel RealSense D405 camera. The first device is already widely used in the literature [19] and has been characterized for close-range acquisitions in a previous work [5]. The D405, on the other hand, is a new model. Both devices use stereo technology for the construction of the 3D point cloud, i.e., triangulation based on correspondences between left and right views along rectified epipolar lines. The differences lie in the fact that the D415 takes advantage of active technology, so it also includes the ability to project a pattern of light onto the scene to help find matches, while the D405 is passive technology, and consequently much more compact, having fewer hardware components. The dimensions of the D405 are 42 mm × 42 mm × 23 mm, the ones of the D415 are 99 mm × 20 mm × 23 mm. Both require a USB 3.0 cable and have a 1/4-20 UNC thread mounting point on the bottom and two M3 thread mounting points on the back.

In an initial test campaign, aimed at choosing which device to use for ear acquisition, the point clouds obtained from the two devices were compared. A calibrated sphere of diameter 25.4 mm, shown in Figure 1, was used for comparison.

Figure 1: Calibrated sphere with diameter equal to 25.4 mm.

Since the depth error of these devices is typically proportional to the distance from the object to be acquired, moving the device closer to the ear region can result in a more accurate acquisition, thus the sphere was first acquired at the minimum possible distance in the default settings for the two devices, which is for the D405 at ~70 mm and for the D415 at ~500 mm. Then, by changing the disparity shift parameter of the two devices, the sphere was acquired at the same distance of ~150 mm. These devices in fact evaluate the depth as a proportional inverse of the pixel disparity from the right image to the left image, where the pixel disparity is evaluated along the rectified

epipolar lines [14] and this depth, called disparity shift, can be varied to change the acquisition range; this allows the D415 device to also acquire in the very-close range. The distance of about 150 mm was chosen to be tested as it allows the device to be held close to the ear anatomy yet not too close, so as to avoid the need for too many acquisitions. The disparity shift value was chosen so that at least +- 20 mm could be acquired with respect to the reference value of 150 mm. This value could be determined using disparity shift graphs such as those presented in [5], i.e., graphs that correlate the disparity shift value with the minimum and maximum acquirable distance.

The acquisitions were repeated 10 times for each device, and two errors were evaluated for each cloud: the difference between the measured and actual sphere diameter, and the deviation from the best-fit sphere. This provided an indication of the spatial accuracy and on the noise introduced on the points by the device. Figure 2 shows one acquisition for each performed test. It can be noticed that the point clouds acquired by the D415 device have a "step-like" appearance, this is due to the default depth unit value of the devices: for the D415, the depth unit value is set at 1000, being a camera designed for the mid-range, while for the D405 it is set at 100. Table 1 shows the results averaged over the 10 acquisitions for the different acquisition distances.

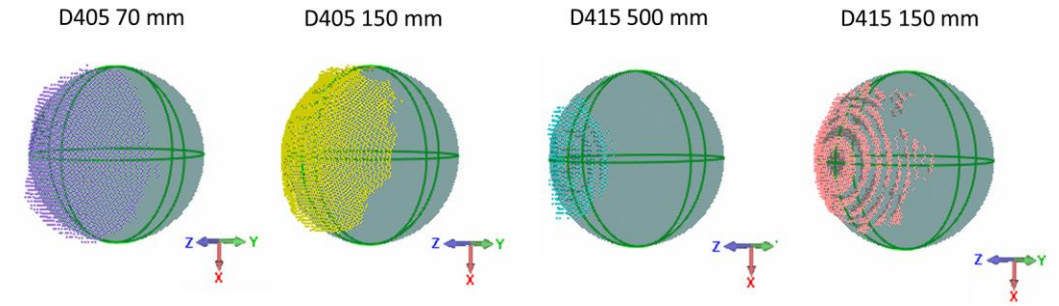

Figure 2: An example of a point cloud acquired for each setup and the relative best-fitting sphere.

Acquisition Device/Distance	*Average diameter error [mm]*	*Average max deviation [mm]*	*Average min deviation [mm]*
D405 - 70 mm	0,4	0,788	-0,236
D415 - 500 mm	8,28	2,264	-1,1448
D405 - 150 mm	0,22	0,724	-0,164
D415 - 150 mm	0,46	1,078	-0,95

Table 1: Average diameter error and deviation error for each experimental setup.

Examining the results shown in Table 1, it can be seen that the acquisitions obtained with the D415 device at the nominal minimum distance are significantly worse than the other results even though they significantly improve when the camera is closer to the subject. In general, the best performance is obtained using the D405 device at ~150 mm distance from the subject. Therefore, it was chosen to proceed the scanner implementation with the D405 device that combines good accuracy when used in the very-close range with very small dimensions.

2.2 Definition of Acquisition Viewpoints

The second step involved establishing the viewpoints required to capture the entire auricular region, thus the possible configurations of multiple devices framing the subject's face so that there are no occlusions in the ear reconstruction. Given the particularity of this anatomical region, which

differs greatly among subjects, a strategy based on texture painting was implemented. The operational flow was as follows: 1) creation of a dataset of 15 sensitively different ears using MakeHuman software [24]; 2) import of the models within Blender software [25] and creation of the texture; 3) definition and placement of the devices; 4) evaluation through the "texture paint" tool of the regions acquired in the specific configuration and of the overlaps between the different views; 5) evaluation of the result with special attention to occlusions and possible repetition of steps 3) and 4).

The MakeHuman software allows to make humanoid models by modifying generic parameters such as gender, age, weight, height, proportions, etc., and then provides the possibility to modify more specific parameters, as far as the ear is concerned these are position, scale, rotation and shape. Biometric values of ear variability reported in the literature were used to make the 15 ear anatomies [11,6]. Figure 3 shows some examples of faces created for this application.

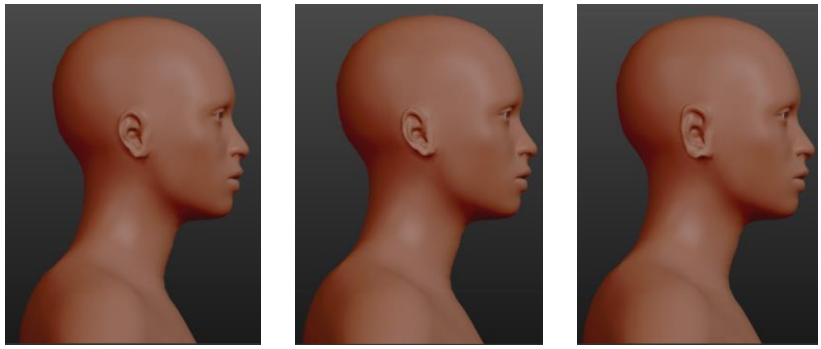

Figure 3: Examples of faces with different ear created with MakeHuman.

The subsequent steps took advantage of the functionalities of Blender software. Each MakeHuman model was imported into the Blender environment and its texture was created. For this purpose, Blender allows for UV mapping, which is a technique that matches three-dimensional coordinates (x, y, z) of mesh points to two-dimensional coordinates (u, v) of a texture image. To create the texture image, the vertices of the anatomical region containing the ear were manually selected (blue highlight in Figure 4) and unfolded in the two-dimensional image (on the left in Figure 4) using the UV mapping operation.

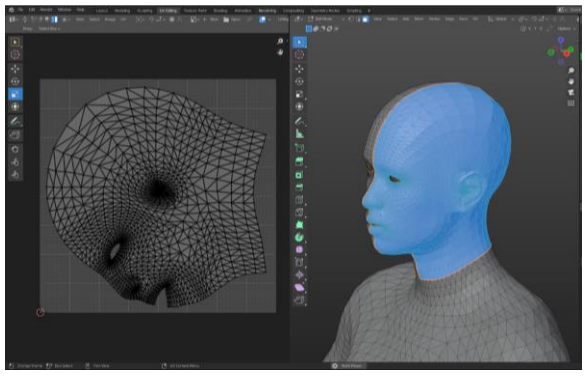

Figure 4: UV mapping of the head within Blender.

The cameras in the Blender environment were generated by inputting the FOV and focal distance of the device. To test a specific configuration, each camera position was used to color the framed portion of the face; different colors were used for each position, thus it was possible to evaluate blind spots in the configuration and areas of overlap, which are important to facilitate the correct alignment of the point clouds.

To define the different configurations to be tested, the origin of the reference system was positioned at the center of the ear and consequently a triplet of Cartesian planes oriented as the three sagittal (YZ plane) transverse (XY plane) and frontal (XZ plane) planes of the subject was created. The transverse and frontal planes were chosen for camera positioning, evaluating for the latter the possible rotations with respect to the Z-axis, and the camera was moved on a sphere of radius 150 mm.

Of all the possible configurations in which it is possible to acquire the whole ear, it was chosen to focus on two configurations that seek to minimize the number of necessary acquisitions while moving the devices on the principal planes: the configuration shown in Figure 5(a) uses 6 devices, 4 on the transverse plane and two in the frontal plane, acquiring anatomy from the bottom and from the top. The cameras placed on the frontal plane are tilted with respect to the x-axis by -45° and 40°, respectively, while those on the transverse plane are tilted by -40°, 0°, 40° and 80°, respectively.

The second configuration, on the other hand, requires 8 viewpoints for full ear acquisition (Figure 5(b)). The cameras are tilted by -40° and 40° with respect to the X-axis and placed in the frontal plane and three other planes resulting from the rotation of the frontal plane with respect to the Z-axis by -40°, 40° and 80°, respectively. Figure 6 shows the result of using the texture paint function in the two configurations, as mentioned above, this feature was used to verify that the acquisition lacked occluded areas; different colors indicate different positions of the cameras, and thus it is possible to verify complete coverage of the anatomical region, and the presence of overlapping points between acquisition. As can be seen in Figure 5, to ensure acquisition of the posterior part of the anatomy, the two configurations are not symmetrical with respect to the ear, so they must be rotated 180° on the Z axis for the acquisition of the contralateral ear.

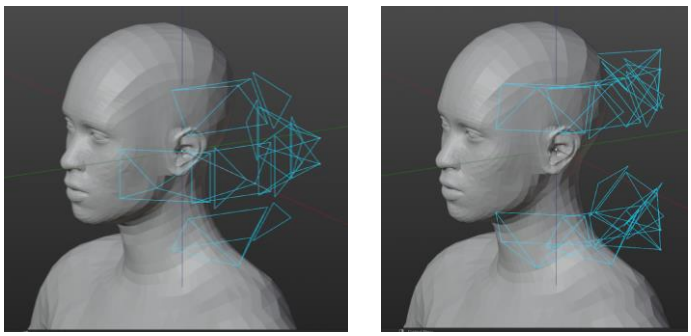

Figure 5: The two configurations analyzed for complete ear acquisition.

Three main factors were considered to choose the solution to be implemented: the cost of the scanner, the manageability, and the acquisition speed. Obviously, the number of used cameras negatively affect the cost and manageability, but positively impact on the acquisition speed.

Combining these factors, it was decided to implement a solution based on the viewpoints shown in the second solution (Figure 5(a)) but using only two devices, moved sequentially to 4 positions by the user, so as to cover the 8 viewpoints. In this way, as shown in the next section, it

was possible to realize a more economical and lightweight scanner (only two devices) with acceptable acquisition times for the specific application, the ear region in fact even following micro movements of the head remains morphologically unchanged.

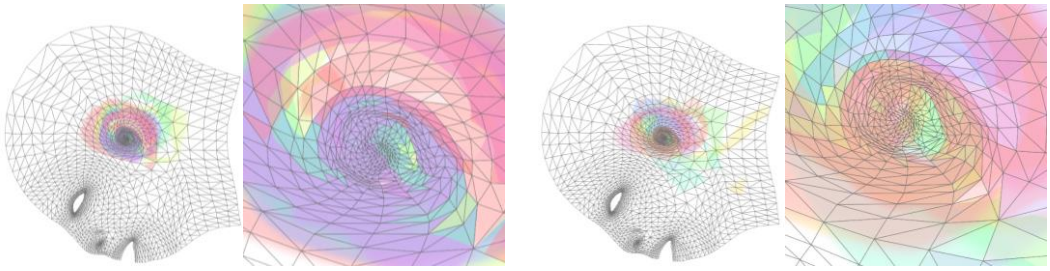

Figure 6: Result of texture paint function for the two configurations.

2.3 Hardware and Software Design

The devised scanner, shown in Figure 7, refers to the second configuration with the idea of positioning 2 cameras at the predetermined angle defined in the above paragraph and then providing for synchronous translation.

An important aspect to consider during the design is the possibility of acquiring both right and left ears, thus, as anticipated in the previous paragraph, the possibility of rotating the system 180° in the Z axis. In addition, it is clearly important that the cameras maintain the position shown in Figure 5 with respect to the head, within small variations, so it is not conceivable to use the scanner while manually holding the structure, therefore a support was devised to keep it in place.

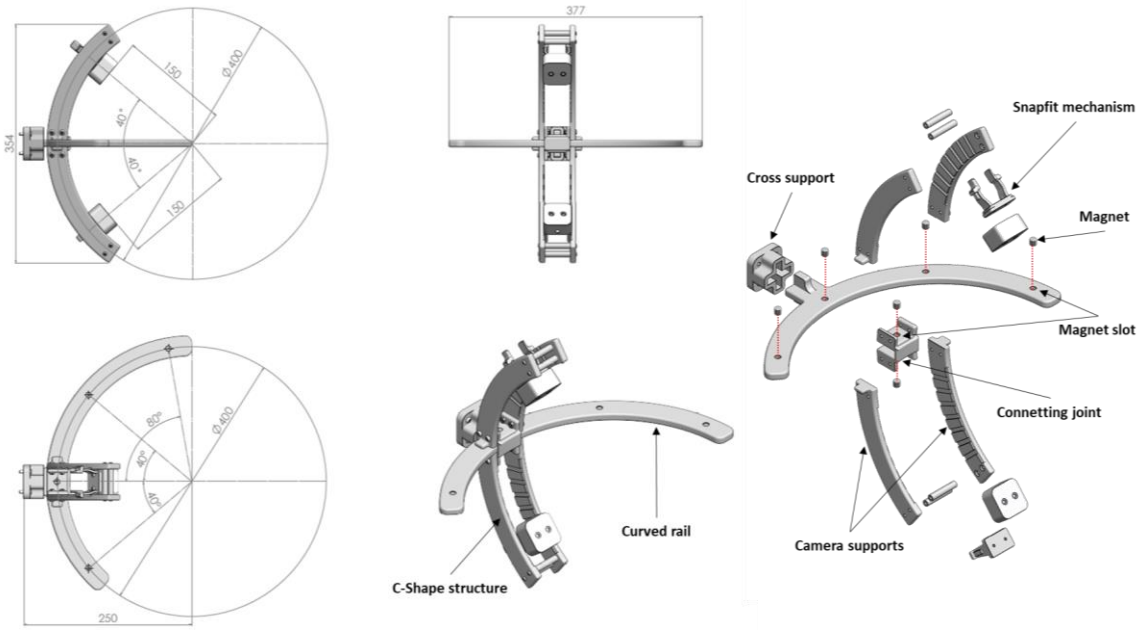

Figure 7: CAD model of the scanner and exploded model.

A C-Shape structure consisting of two camera supports and a connecting joint was constructed to ensure manual translation. Movement in the four positions identified above was achieved by sliding the C-shape structure on a curved rail. Two 400-mm-diameter curved supports were made to hold the cameras in position. These were joined at the top by cylindrical spacers and at the bottom by a connecting joint. The joint was designed to function as a slide and slide along the 400-mm-diameter curved rail. The joint was designed to be placed in contact with the upper and lower surfaces of the rail and has a cylindrical shape internally to be tangent to the lateral surface during translation. In order to be able to quickly move the C-shaped structure to the 4 positions, 2 holes have been provided on the connecting joint and 4 holes on the rail.

Four magnets in the curved rail (in red) and two in the connecting joint (in green) were respectively inserted into the dedicated holes, oriented with the same polarity. Thanks to these magnets the system can be block in position to perform acquisitions.

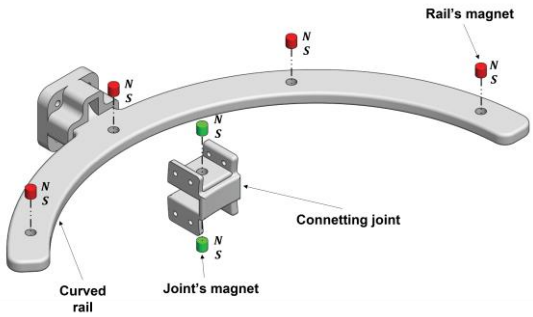

Figure 8: Positioning of magnets on the curved rail and on the connecting joint.

Since the configurations obtained with Blender refer to biometric ear values defined in previous studies, it was considered that in order to maximize the manageability and scalability of the system, thus to prepare it for possible dimensions that deviate from the average, the acquisition devices are hold with snap-fits mechanism that allow the device to be moved manually with a +-5° step (for a total variation of min 15° and max 45° from the horizontal axis).

To hold the scanner in the correct position with respect to the patient's face, a cross-shaped wall support was provided in which the circular guide can be rotated 180° in order to perform acquisition of both right and left ears. The rotation is depicted in Figure 9.

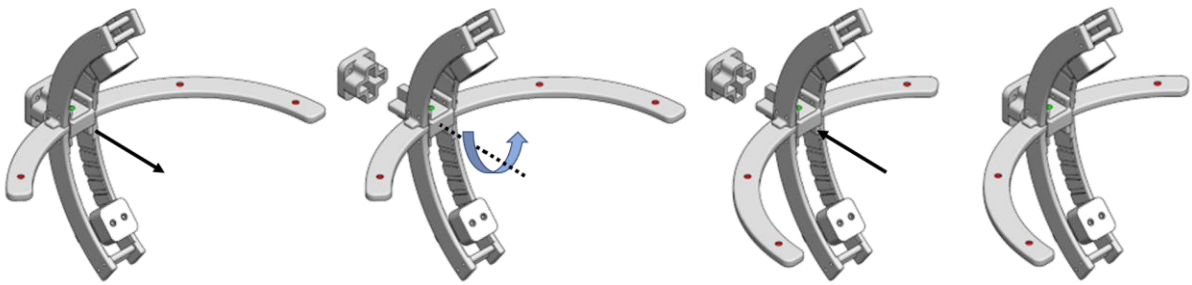

Figure 9: Rotation of the curved rail to acquire left and right ears.

In addition, a mount compatible with photo tripods was also realized to provide a stable solution while allowing more freedom for the operator in positioning the scanner.

All components were designed to be manufactured with the Fortus F370 3D printer (print plate size 355x254x355 mm), Figure 10.

Figure 10: Ear scanner manufactured with Fortus F370 3D printer.

A software interface was associated with the scanner providing the user with the ability to start the scan and view the result (Figure 11). The program was implemented in C++ using the librealsense2 library API provided by Intel to turn on the devices and acquire the point clouds. For each position of the camera pair, the software performs the acquisition and notifies the user via audio, so that the operator can move the cameras to the next position within 2 s, as described above. The total scan therefore takes ~10 s and once all point clouds are obtained they are processed with point cloud library (PCL) functions [18]. Specifically, the point clouds are trimmed to isolate the region of interest, cleaned with noise removal and smoothing operations, and finally merged with two alignment steps. A first coarse alignment is based on the known mutual position of the 8 acquisitions, it is in fact possible to move all the point clouds to the same reference system since the mutual positions of the devices are known a priori. This first alignment then needs to be refined with an ICP step since small reciprocal movements between the patient and the scanner are likely to occur during the acquisition. The coarse alignment is refined with the ICP algorithm by iteratively aligning each scan to the other seven.

Figure 11: User interface devised to operate the scanner.

3 RESULTS

To test the system, an evaluation strategy was devised that could consider both the quantitative aspect, thus the accuracy of the acquisition, and the qualitative aspect, thus the usability and handling of the system.

The quantitative aspect involved ear acquisitions of four subjects with both the proposed scanner and the high-precision Artec Spider scanner. The acquisitions were compared by evaluating the deviation between the reference geometry and the scanned anatomy using Geomagic Design X, after aligning them with the ICP algorithm provided by the software. Two examples are shown in Figure 12, and the deviation values obtained are shown in Table 2.

	Average deviation [mm]	***Max deviation [mm]***	***Min deviation [mm]***
S1	0.09	2.79	-2.24
S2	0.047	2.39	-2.38
S3	0.016	2.49	-2.49
S4	0.025	2.73	-2.71

Table 2: Deviation between the acquisitions performed with the proposed scanner and the Artec Spider on four subjects.

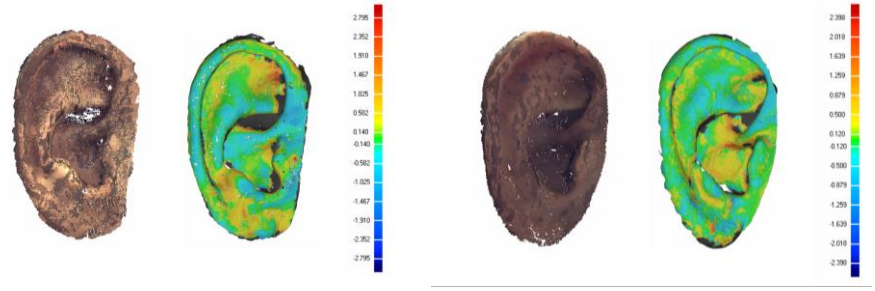

Figure 12: Deviation between ear acquisition with the proposed scanner and the Artec Spider on two subjects.

For the utilization test the scanner was used by three physicians and a simple standardized SUS questionnaire [7] was prepared to evaluate the appreciation of the system. The results of the SUS questionnaire are shown in Figure 13, where the values below the purple dashed line are to be considered highly insufficient, the yellow line indicates the threshold of sufficiency, and the results above the green line are to be considered optimal. The scanning system achieved an average score of 90, and all scores are above the green line which indicates a high overall level of user satisfaction.

4 CONCLUSION

In recent years, a disruptive interdisciplinarity characterized by collaboration between clinicians and engineers has been observed. This phenomenon pivots partly on modern RE and AM technologies that allow revisiting and modernizing some established treatment strategies, in the direction of achieving strong therapy personalization. In this context, however, it is also important to focus on how medical staff can fully exploit these new technologies, and to develop tools that are accessible and user-friendly. To this end, this work proposes a new scanner designed to acquire auricular anatomy in a simple and efficient way. The design of the scanner was based on balancing several factors, such as cost, bulk, and acquisition speed, which is especially important in pediatric

settings. The result is a device consisting of two low-cost depth cameras that slide on a guide that moves around the patient's ear to acquire it in 360°, controlled through a simple software interface. The system was tested on four subjects obtaining average deviations of ~0.05 mm with the range of error always within 3 mm. In addition, the satisfaction with the system was evaluated by having 3 physicians use it, and then filling out a SUS questionnaire. As a result, the device obtained an average questionnaire grade of 90, largely above the highest threshold. Future developments include using the scanner to acquire the healthy ear of patients affected by microtia and using the scan to make medical devices that can help the surgeon in preoperative planning and simulation of the restorative surgery.

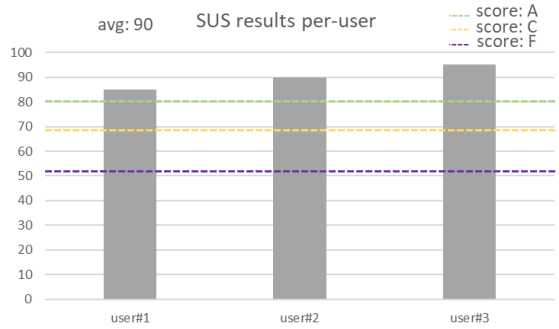

Figure 13: Results of the SUS questionnaire.

Michaela Servi, https://orcid.org/0000-0002-4071-6615
Elisa Mussi, https://orcid.org/0000-0002-5170-3246
Andrea Profili, https://orcid.org/0000-0002-1727-1013
Yary Volpe, https://orcid.org/0000-0002-5668-1912

REFERENCES

[1] Ahangar, P.; Cooke, M.E.; Weber, M.H.; Rosenzweig, D.H.: Current Biomedical Applications of 3D Printing and Additive Manufacturing, Applied Sciences, 9, 2019, 1713. https://doi.org/10.3390/APP9081713

[2] Ahn, M.S.; Chae, H.; Noh, D.; Nam, H.; Hong, D.: Analysis and Noise Modeling of the Intel RealSense D435 for Mobile Robots; 16th International Conference on Ubiquitous Robots (UR), 2019. https://doi.org/10.0/Linux-x86_64

[3] Baluch, N.; Nagata, S.; Park, C.; Wilkes, G.H.; Reinisch, J.; Kasrai, L.; et al.: Auricular reconstruction for microtia: A review of available methods, 22, 2014, 39–43. https://doi.org/10.1177/229255031402200102

[4] Buonamici, F.; Furferi, R.; Governi, L.; Lazzeri, S.; McGreevy, K.S.; Servi, M.; Talanti, E.; Uccheddu, F.; Volpe, Y.: A Practical Methodology for Computer Aided Design of Custom 3D Printable Casts for Wrist Fractures, The Visual Computer, 36, 2018, 375–390. https://doi.org/10.1007/s00371-018-01624-z

[5] Carfagni, M.; Furferi, R.; Governi, L.; Santarelli, C.; Servi, M.; Uccheddu, F.; Volpe, Y.: Metrological and critical characterization of the intel D415 stereo depth camera, Sensors, 19(3), 2019, 489. https://doi.org/10.3390/s19030489

[6] Fu, F.; Luximon, Y.: A systematic review on ear anthropometry and its industrial design applications, Human Factors and Ergonomics In Manufacturing, 30, 2020, 176–194. https://doi.org/10.1002/HFM.20832

[7] Grier, R.A.; Bangor, A.; Kortum, P.; Peres, S.C.: The System Usability Scale: Beyond Standard Usability Testing, Proceedings of the Human Factors and Ergonomics Society 57th Annual Meeting 2013. https://doi.org/10.1177/1541931213571042

[8] Guidi, G.; Gonizzi, S.; Micoli, L.: 3d capturing performances of low-cost range sensors for mass-market applications, ISPRS - International Archives of the Photogrammetry, Remote Sensing and Spatial Information Sciences, XLI-B5, 2016, 33–40. https://doi.org/10.5194/isprsarchives-XLI-B5-33-2016
[9] Han, J.; Shao, L.; Xu, D.; Shotton, J.: Enhanced Computer Vision with Microsoft Kinect Sensor: A Review, IEEE transactions on cybernetics, 43, 2013. https://doi.org/10.1109/TCYB.2013.2265378
[10] Hausamann, P.; Sinnott, C.B.; Daumer, M.; Macneilage, P.R.: Evaluation of the Intel RealSense T265 for tracking natural human head motion, Scientific Reports |, 11, 123AD, 12486. https://doi.org/10.1038/s41598-021-91861-5
[11] Jha, A.; Sara Mundappallil Jacob, N.; Mathew, S.; Kumar Handigodu Duggappa, A.; Muhamed, S.; Udupi, S.: A randomized controlled trial to compare the auricle size-based method for ProSeal laryngeal mask airway selection with the weight-based method among paediatric patients, Trends in Anaesthesia and Critical Care, 37, 2021, 50–54. https://doi.org/10.1016/J.TACC.2020.08.004
[12] Kidane, N.; Shen, Y.; Kelly, R.E.: Optical Imaging for Monitoring Pectus Excavatum Therapy; IEEE International Conference on Bioinformatics and Biomedicine (BIBM), 2021. https://doi.org/10.1109/BIBM52615.2021.9669543
[13] Lain, A.; Garcia, L.; Gine, C.; Tiffet, O.; Lopez, M.: New methods for imaging evaluation of chest wall deformities, Frontiers in Pediatrics, 5, 2017, 257. https://doi.org/10.3389/fped.2017.00257
[14] Morgan, G.L.K.; Liu, J.G.; Yan, H.: Precise Subpixel Disparity Measurement From Very Narrow Baseline Stereo, IEEE Transactions on Geoscience and Remote Sensing, 48, 2010, 3424–3433. https://doi.org/10.1109/TGRS.2010.2046672
[15] PA, F.: Auricular Prostheses in Microtia, Facial Plastic Surgery Clinics of North America, 26, 2018, 97–104. https://doi.org/10.1016/J.FSC.2017.09.007
[16] Patil Preeti Bailke, J. V: Real time facial expression recognition using RealSense camera and ANN; International Conference on Inventive Computation Technologies (ICICT), 2016. https://doi.org/10.1109/INVENTIVE.2016.7824820
[17] Romo, T.; Reitzen, S.D.: Aesthetic microtia reconstruction with medpor, Facial Plastic Surgery, 24, 2008, 120–128. https://doi.org/10.1055/S-2008-1037453/ID/27
[18] Rusu, R.B.; Cousins, S.: 3D is here: Point Cloud Library (PCL), 2011 IEEE International Conference on Robotics and Automation, 2011, 1–4. https://doi.org/10.1109/ICRA.2011.5980567
[19] Servi, M.; Mussi, E.; Profili, A.; Furferi, R.; Volpe, Y.; Governi, L.; et al.: Metrological Characterization and Comparison of D415, D455, L515 RealSense Devices in the Close Range, 21(22), 2021, 7770. https://doi.org/10.3390/s21227770
[20] Stephenson, K.: A Detailed Five-Year Review of Medical Device Additive Manufacturing Research and its Potential for Translation to Clinical Practice, Proceedings of the ASME Design Engineering Technical Conference, 3, 2016. https://doi.org/10.1115/DETC2015-47671
[21] Yamada, A.; Imai, K.; Fujimoto, T.; Morimoto, K.; Niitsuma, K.; Matsumoto, H.: New training method of creating ear framework by using precise copy of costal cartilage, Journal of Craniofacial Surgery, 20, 2009, 899–902. https://doi.org/10.1097/SCS.0b013e3181a2ef97
[22] Yang, K.; Wang, K.; Hu, W.; Bai, J.: Expanding the Detection of Traversable Area with RealSense for the Visually Impaired, Sensors, 16(11), 2016, 1954. https://doi.org/10.3390/s16111954
[23] Zhou, J.; Pan, B.; Yang, Q.; Zhao, Y.; He, L.; Lin, L.; et al.: Three-dimensional autologous cartilage framework fabrication assisted by new additive manufactured ear-shaped templates for microtia reconstruction, Journal of Plastic, Reconstructive and Aesthetic Surgery, 69, 2016, 1436–1444. https://doi.org/10.1016/J.BJPS.2016.06.011
[24] www.makehumancommunity.org. (accessed: 01/10/2022)
[25] www.blender.org - Home of the Blender project - Free and Open 3D Creation Software. (accessed: 01/10/2022)